Editors' Suggestion

Exceptional Points of *PT*-Symmetric Reflectionless States in Complex Scattering Systems

Clément Ferise,[1] Philipp del Hougne,[1] Simon Félix,[2] Vincent Pagneux,[2] and Matthieu Davy[1,*]
[1]*Univ Rennes, CNRS, IETR-UMR 6164, F-35000 Rennes, France*
[2]*Laboratoire d'Acoustique de l'Université du Mans (LAUM), UMR 6613, Institut d'Acoustique - Graduate School (IA-GS), CNRS, Le Mans Université, France*

(Received 28 October 2021; accepted 19 April 2022; published 20 May 2022)

We investigate experimentally and analytically the coalescence of reflectionless (RL) states in symmetric complex wave-scattering systems. We observe RL exceptional points (EPs), first with a conventional Fabry-Perot system for which the scattering strength within the system is tuned symmetrically and then with single- and multichannel symmetric disordered systems. We confirm that an EP of the parity-time (*PT*)-symmetric RL operator is obtained for two isolated quasinormal modes when the spacing between central frequencies is equal to the decay rate into incoming and outgoing channels. Finally, we leverage the transfer functions associated with RL and RL-EP states to implement first- and second-order analog differentiation.

DOI: 10.1103/PhysRevLett.128.203904

Exceptional points (EPs) are spectral singularities in non-Hermitian systems at which two or more eigenvalues and eigenstates coalesce [1–5]. EPs have mainly been explored for resonant states that are the poles of the scattering matrix and scattering states. In systems with losses but no gain, finding an EP between two resonant modes requires that the mutual coupling between resonances satisfy a critical relation with their loss factors [6]. EPs are, however, more easily realizable in systems with *PT* symmetry obtained by balancing gain and loss in symmetric regions [6,7]. Many unconventional features of EPs have been demonstrated theoretically and experimentally such as the design of unidirectional invisibility [8,9], asymmetric mode switching [10], or directional lasing [11], to cite a few (see Refs. [6,12] for reviews). These spectral singularities are also interesting for sensing applications, since the energy (or frequency) splitting between n degenerate eigenstates scales as the nth root of the perturbation [13,14].

Recently, a new kind of EPs associated with reflectionless (RL) scattering states rather than resonances has been investigated [15–19]. RL states are eigenstates of a non-Hermitian operator H_{RL} based on the wave equation with incoming channels connected to a scattering system modeled as gain and outgoing channels modeled as losses [16,17,20–22]. The eigenvalues $\tilde{\omega}_R$ of H_{RL} are distinct from the resonance spectra related to the poles of the scattering matrix $S(\omega)$. When an eigenvalue is tuned to the real axis, the corresponding RL state enables reflectionless coupling of incoming channels. The excitation of RL states in multichannel systems requires appropriate wave-front shaping [23,24].

A special case of RL EPs found for purely incoming boundary conditions is the coalescence on the real axis of two zeros of the complete scattering matrix $S(\omega)$ known as a perfectly absorbing EP [18,19,25]. The phenomenon of coherent perfect absorption (CPA) occurs when absorption within a scattering medium balances the excitation rate of incoming channels [26–29]. CPA is the time reverse of lasing at threshold [23,30] and a generalization of the critical coupling condition [28,31]. CPA has been observed in a wide range of regular scattering systems [32], as well as in disordered matter [33–39]. Disordered matter can be tuned *in situ* to impose a real-valued scattering zero at a desired frequency, as reported in Ref. [33] and subsequently generalized to multiple channels [35,36], to additional constraints on the CPA wave front [37], or to multiple simultaneous real-valued zeros [39]. When two CPA states coalesce, the broadened line shape of the absorption spectrum indicates the existence of perfectly absorbing EPs [18,19,25].

In flux-conserving systems, the probability of finding RL scattering modes with zero reflection and, therefore, perfect transmission is naturally enhanced in scattering systems with mirror symmetry for which the RL operator is *PT* symmetric and RL eigenvalues feature an exciting property. An RL eigenvalue remains on the real axis under continuous perturbation of the system until it coalesces with a second one at an EP before splitting into a complex-conjugate pair [17,18,22]. The spectral broadening of the transmission peak corresponding to RL EPs has been observed in ac filters at the Butterworth condition [40,41], in multimirror cavities [42–44], and in numerical simulations of quantum dots [45] and atomic wires [46], though not interpreted as an EP. However, while isolated RL states can be analyzed within the framework of quasinormal modes using the coupled mode theory (CMT) [19], a clear experimental demonstration of RL

 © 2022 American Physical Society

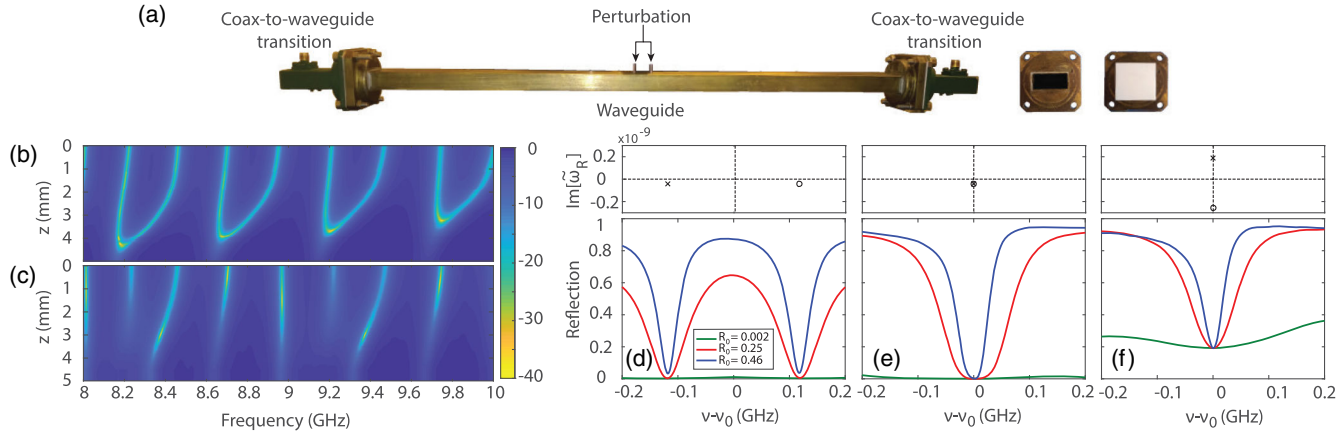

FIG. 1. (a) Experimental setup. The penetration depth z of two symmetrical rods can be finely controlled with a translation stage. Inset: a channel (coax-to-waveguide transition) with an empty opening or with an alumina slab placed in front to increase the reflectivity at the waveguide interfaces. (b),(c) Color scale representation of the reflection on a decibel scale, $10\log[R(\nu,z)]$, measured with a vector network analyzer between 8 and 10 GHz for a symmetric (b) and an asymmetric (c) perturbation. RL EPs appear when two branches with $R\sim 0$ shown in yellow coincide. (d)–(f) $R(\nu,z)$ in the underperturbed $z<z_{\mathrm{EP}}$ (d), critically perturbed $z=z_{\mathrm{EP}}$ (e), and overperturbed $z>z_{\mathrm{EP}}$ (f) regimes as a function of rescaled frequency $\nu-\nu_0$ ($\nu_0=8.2$ GHz). Spectra are shown for zero (green line), one (red line), and two (blue line) dielectric slabs at each interface. The corresponding RL eigenvalues $\tilde{\omega}_{R\pm}$ found from Eq. (2) are shown on the top in the complex plane. They coalesce at complex frequencies with a small imaginary part resulting from absorption $\mathrm{Im}[\omega_{R\pm}]=-\gamma_a$, with $\gamma_a=30$ MHz.

EPs in disordered systems and an analysis in terms of complex resonances has to date not been reported.

In this Letter, we experimentally observe the existence of RL EPs in symmetric regular and disordered systems that are tuned toward this scattering anomaly by inserting a symmetric defect. While our experimental system has a measurable degree of absorption, it is small enough to clearly observe the coalescence of two RL states. We start with a multimirror Fabry-Perot cavity for which the reflectivity at the center is progressively increased. Our harmonic analysis reveals that an RL EP is obtained for two overlapping resonances when the spacing between the central frequencies is equal to their linewidth. Our experimental results in the microwave range are in excellent agreement with the CMT that describes the coupling of these two resonances [19]. We then demonstrate RL EPs in disordered single- and multichannel waveguides. Finally, we show that designing systems operating at an RL EP is relevant to analog computations of derivatives.

We measure spectra of the reflection coefficient $r(\nu)$ and the transmission coefficient $t(\nu)$ through a single-mode rectangular waveguide supporting only the fundamental transverse-electric mode between 7 and 11 GHz (length $L=400$ mm, width $W=22.86$ mm, and height $H=10.16$ mm) with two coax-to-waveguide transitions attached to the openings [see Fig. 1(a)]. A dielectric alumina slab of reflectivity $R_0=0.25$ (see Supplemental Material [47]) is positioned between each transition and the waveguide to increase the internal reflection at the interfaces. A perturbation is introduced symmetrically with respect to the center of the waveguide by inserting two aluminum rods (diameter 2 mm) through two holes drilled into the top plate and spaced by 12 mm. The penetration depth z varies from 0 to 8 mm in steps of $\Delta z=0.02$ mm ($\Delta z\sim\lambda/1666$). This system is, therefore, equivalent to a multimirror Fabry-Perot interferometer with tunable reflectivity at the center.

A color map of the reflection $R(\nu,z)=|r(\nu,z)|^2$ is shown in Fig. 1(b) on a logarithmic scale. In the absence of the perturbation ($z=0$), the frequencies corresponding to extremely small reflection (bright area) are regularly spaced. As the penetration depth z increases, the RL frequencies move closer until they coalesce for a critical perturbation ($z=z_{\mathrm{EP}}$). The two peaks on the spectrum of $R(\nu)$ found in the underperturbed regime ($z<z_{\mathrm{EP}}$) transform into a single broadband one at z_{EP} with a flattened quartic line shape which is characteristic of EPs [18,19,25,39]. Once two RL eigenvalues have collapsed, they leave the real axis as complex-conjugate pairs. In the overperturbed regime $z>z_{\mathrm{EP}}$, the minimum of $R(\nu)$ increases with z as the imaginary part of RL eigenvalues moves away from the real axis. In contrast, for an asymmetrical perturbation of the Fabry-Perot cavity (a single rod inserted at $x=L/4$), the zero-reflection frequencies do not collapse but move independently in the complex plane [see Fig. 1(c)].

The same procedure is then repeated for samples without an alumina slab and with two alumina slabs at each interface, yielding $R_0=0.002$ and $R_0=0.46$, respectively. For the smallest R_0, the reflectivity is solely due to the small impedance mismatch between the transitions and the waveguide. In each case, a symmetric perturbation leads

to the formation of RL EPs. The linewidth of resonances decreases with increasing R_0, and the spectral dips corresponding to RL states narrow as seen in Figs. 1(d)–1(f).

We now analyze RL eigenvalues found by tracking the local minima of $R(\omega, z)$ in terms of quasinormal modes that are solutions of the wave equation with purely outgoing boundary conditions (i.e., for *both* left and right channels). The eigenstates $\psi_n(x)$ are associated with complex frequencies $\tilde{\omega}_n = \omega_n - i\Gamma_n/2$ with central frequency ω_n and linewidth Γ_n. We extract the set of complex frequencies $\tilde{\omega}_n$ from a modal analysis of transmission spectra between 7 and 11 GHz using the harmonic inversion method [51,52] (see Supplemental Material [47]). In the absence of perturbation, the central frequencies almost coincide with RL frequencies. However, for $z = z_{\mathrm{EP}}$, two overlapping resonances mainly contribute to the flattened transmission peak as seen in Fig. 2(a). Two peaks are observed on the spectrum of the density of states (DOS) $\rho = (1/2\pi)\Sigma_n(\Gamma_n/2)/[(\omega-\omega_n)^2 + (\Gamma_n/2)^2]$ in Fig. 2(b) with a spacing between central frequencies approximately given by the linewidths. This confirms experimentally that, in three-mirror resonators, RL EPs are associated with two noncoalescing resonances as expected from the relation to Butterworth filters [40] and from numerical results [17]. Even for the highest penetration depth of the rods, the resonances do not merge.

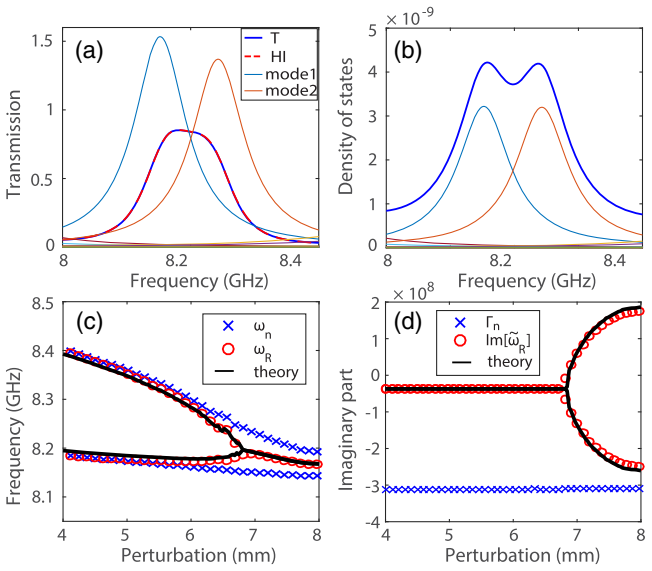

FIG. 2. (a) Modal analysis of the transmission coefficient $t(\nu, z_{\mathrm{EP}})$. Two modes with lines shown in orange and cyan mainly contribute to $T = |t(\nu, z_{\mathrm{EP}})|^2$ (blue line), which is perfectly reconstructed from harmonic inversion (red dashed line). The maximum transmission is below unity $T_{\max} = 0.87$ due to non-negligible absorption. (b) The DOS presents two peaks corresponding to the maxima of the two resonances. (c),(d) Real (c) and imaginary (d) parts of the reflectionless eigenvalues (red circles) and eigenfrequencies (blue crosses) with respect to z. The black lines are the theoretical values of $\tilde{\omega}_R$ found from Eq. (2) with the values of $\omega_n(z)$ and $\gamma(z)$.

To further confirm that the coalescence of zeros on $R(\nu)$ forms an RL EP, we now derive analytical expressions for $\tilde{\omega}_n$ and RL eigenvalues $\tilde{\omega}_R$ using standard CMT [19]. The effective Hamiltonian H_{eff} of the open system is expressed in the basis of two successive modes of a closed one-dimensional waveguide, $H_{\mathrm{eff}} = H_0 - iV_0V_0^T/2 - iV_1V_1^T/2$, with H_0 being a diagonal matrix with elements $\omega_0 - \delta\omega_0/2$ and $\omega_0 + \delta\omega_0/2$. The left and right vectors V_0 and V_1 account for the coupling of the closed system to the channels and are real for systems with time-reversal symmetry. The scattering matrix is written $S(\omega) = 1 - iV^T[\omega\mathbb{1} - H_{\mathrm{eff}}]^{-1}V$, where $V = [V_0; V_1]$. For an empty one-dimensional cavity of length L, the nth eigenfunction of the closed systems is $\psi_n(x) = (2/L)\sin(n\pi x/L)$. Because the EPs in our system result from the overlap of two resonances with high quality factors, we restrict our analysis to a two-level Hamiltonian as previously done in Ref. [19] for a CPA EP. We, consider an even resonance [$n \equiv 0 \pmod 2$] and an odd resonance [$n \equiv 1 \pmod 2$]. The coupling vectors are related to the derivative of $\psi_n(x)$ at $x = 0$ and $x = L$. V_0 is, therefore, symmetric, $V_0 = \sqrt{\gamma/2}(11)$, and V_1 is antisymmetric, $V_1 = \sqrt{\gamma/2}(1-1)$. The coupling rate $\gamma/2$ of each channel to the cavity depends on the reflectivity at the interfaces of the waveguide. The effective Hamiltonian is, therefore, a diagonal matrix with eigenvalues $\tilde{\omega}_{M\pm} = \omega_0 \pm \delta\omega_0/2 - i\gamma/2$ (see Supplemental Material [47]).

Inserting a rod in the middle of the waveguide leads to a local change $\Delta\epsilon(x = L/2)$ of the permittivity. At first order, the frequency shift of a resonance is $\Delta\omega_n \propto -\Delta\epsilon(x)|\psi_n(x)|^2$ [53,54]. For even resonances, the field cancels at the center of the waveguide and $\Delta\omega_n \sim 0$. For odd resonances, $|\psi_n(x)|^2 \neq 0$ and the central frequency shifts toward smaller values. As the penetration depth increases, resonances come together in pairs with central frequencies and spacings that are functions of z, $\omega_0(z)$, and $\delta\omega_0(z)$.

RL modes are eigenvalues of the PT-symmetric operator $H_R = H_0 + iV_0V_0^T/2 - iV_1V_1^T/2$, where an effective gain is associated to incoming channels at the left interface. The coupling of the channels now results in antidiagonal terms $i\gamma$:

$$H_R = \omega_0(z)\mathbb{1} + \frac{1}{2}\begin{pmatrix} -\delta\omega_0(z) & i\gamma \\ i\gamma & \delta\omega_0(z) \end{pmatrix}. \tag{1}$$

The RL eigenvalues $\tilde{\omega}_R$ are then found from a diagonalization of H_{RL}:

$$\tilde{\omega}_{R\pm} = \omega_0(z) \pm \frac{1}{2}\sqrt{\delta\omega_0(z)^2 - \gamma^2}. \tag{2}$$

Uniform absorption within the waveguide is incorporated by adding an imaginary part $-i\gamma_a$ to complex frequencies.

We estimate from the modal analysis that $\gamma_a = 30$ MHz (see Supplemental Material [47]).

When the coupling is small compared to the spacing, $\gamma \ll \delta\omega_0$, RL eigenvalues are real and coincide with the central frequencies of resonances ω_n. However, the spacing between RL eigenvalues decreases more rapidly than $\delta\omega_0(z)$ as the perturbation strength is symmetrically tuned. A reflectionless EP is found when losses through channels are equal to the spacing between the two resonances, $\delta\omega_0(z_{\mathrm{EP}}) = \gamma$. For larger perturbations, the two RL eigenvalues become a complex-conjugate pair. Assuming that $\delta\omega_0(z)$ scales linearly with the penetration depth z near the EP, $\delta\omega_0(z) = \gamma + \kappa/2(z_{\mathrm{EP}} - z)$ (see Supplemental Material [47]), gives a splitting between RL eigenvalues for $z < z_{\mathrm{EP}}$ near the EP $\tilde{\omega}_{R+} - \tilde{\omega}_{R-} \sim \sqrt{\gamma\kappa(z_{\mathrm{EP}} - z)}$ which is characteristic of the square-root detuning behavior of EPs under small perturbations. The same splitting is found on imaginary parts of $\tilde{\omega}_R$ for $z > z_{\mathrm{EP}}$.

The experimental results in Fig. 2(c) for $\mathrm{Re}[\tilde{\omega}_R]$ are in excellent agreement with the prediction of Eq. (2) in which we use the values of $\omega_0(z)$, $\gamma(z)$, and $\delta\omega_0(z)$ extracted from the modal analysis. This agreement also highlights the effectiveness of the coupled mode theory. For $z < z_{\mathrm{EP}}$, the imaginary part of $\tilde{\omega}_R$ is equal to the absorption decay rate $\Gamma_R = -\gamma_a$. For $z > z_{\mathrm{EP}}$, we fit $R(\omega = \omega_0)$ using the following analytical expression for the reflection coefficient (see Supplemental Material [47] for the derivation):

$$r = \frac{[\omega - \omega_0(z)]^2 + [\gamma^2 - \delta\omega_0(z)^2]/4}{[\omega - \omega_0(z)]^2 - [\delta\omega_0(z)^2 + \gamma^2]/4 + i\gamma[(\omega - \omega_0(z)]} = \frac{(\omega - \tilde{\omega}_{R+})(\omega - \tilde{\omega}_{R-})}{(\omega - \tilde{\omega}_{M+})(\omega - \tilde{\omega}_{M-})} \tag{3}$$

and obtain excellent agreement for $\mathrm{Im}[\tilde{\omega}_R]$ in Fig. 2(d).

A signature of an EP is the flattening of $R(\omega)$ close to $\omega = \omega_0(z_{\mathrm{EP}})$ [19,25]. Equation (3) demonstrates that $R(\omega)$ scales as $R(\omega) \sim [\omega - \omega_0(z_{\mathrm{EP}})]^4/\gamma^4$ at an EP and, therefore, features a quartic line shape. This is confirmed in reflection in Fig. 1(e) and in transmission in Fig. 2(a).

RL EPs are not restricted to regular systems but exist in any complex multiple-scattering system. We now add a symmetric disorder made of 28 metallic spheres of diameter 5 mm within the empty waveguide [see Fig. 3(a)]. The spacing between two spheres on the left side is drawn from a uniform random distribution, and we replicate this disorder with a mirror symmetry on the right side. The spectrum $R(\nu)$ still presents clear dips corresponding to RL states, but the spacing between two dips is now random. As the perturbation is symmetrically inserted, pairs of these dips collapse to give rise to RL EPs. z_{EP} is also a random variable which reflects the random field distribution within the waveguide. In contrast to the Fabry-Perot cavity case, however, not all RL eigenvalues are on the real axis for $z = 0$. An interesting case is the variation of RL states

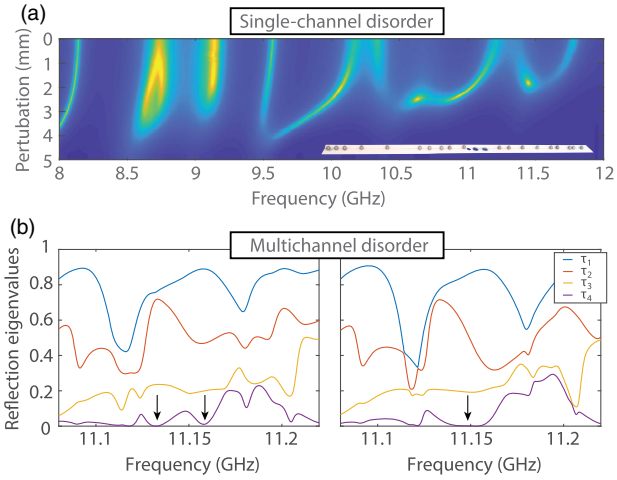

FIG. 3. (a) Color scale representation of $R(\nu, z)$ for a symmetric single-channel disordered medium. The inset shows a picture of metallic spheres inserted within the waveguide. (b) Spectra of reflection eigenvalues $[\tau_1(\nu), \ldots, \tau_4(\nu)]$ in a multichannel disordered cavity in the underperturbed regime (left) and tuned at an RL EP (right). The arrows indicate the frequency of the coalescing zeros of $\tau_4(\nu)$.

around 8.73 GHz. Two eigenvalues first split at an EP for $z = 1$ mm, move away along the real axis, and then come back together to form a second EP for $z = 3.8$ mm.

We also realize an RL EP in a symmetric multichannel systems in the regime of strongly overlapping resonances. Two arrays of $N = 4$ transitions operating between 11 and 16 GHz are attached to an effectively two-dimensional rectangular cavity with metallic boundary conditions of length $L = 0.5$ m, width $W = 0.25$ m, and height $h = 8$ mm (see Refs. [55,56] and Supplemental Material [47] for details). Spectra of the $N \times N$ reflection matrices $r(\nu)$ are measured at both the left and right interfaces of the cavity. The cavity is made disordered with six aluminum rods symmetrically placed on each side of the cavity. By tuning the penetration depth of two rods, we identify an RL EP on the last eigenvalue $\tau_4(\nu, z)$ of $r^\dagger r$ at 11.15 GHz. The two zeros of $\tau_4(\nu, z)$ coalesce at the RL EP with a characteristic quartic line shape [see Fig. 3(b) and Supplemental Material [47] for the color scale representation].

The nontrivial incident wave front v_R corresponding to an RL state is given by the eigenvector of $r^\dagger r$ with the smallest (near-zero) eigenvalue [24]. When the spacing δ between two zeros is large, the corresponding eigenvectors are independent. Their degree of correlation $C = |v_{R+} v_{R-}^\dagger|$ is equal to 0.55 for $\delta = 0.03$ GHz. In contrast to diabolical point with nondegenerate states [4], the eigenvectors become strongly correlated with $C \to 1$ as the two RL states coalesce. A single eigenvalue $\tau_4(\nu, z)$ with a flattened shape is close to zero, and no decrease is observed on $\tau_3(\nu, z)$.

Finally, we note that the transfer functions $r(\nu)$ associated with an RL state and an RL-EP state in reflection

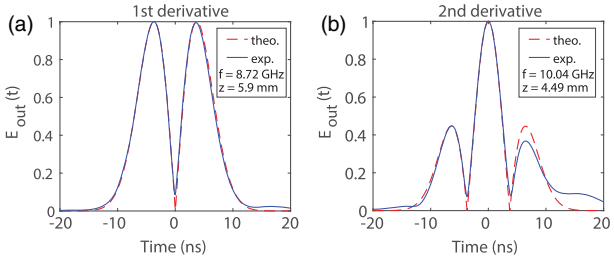

FIG. 4. Analog differentiation of first (a) and second (b) order of a Gaussian pulse (45 MHz bandwidth), simulated based on the transfer function in reflection associated with an RL state and an RL-EP state, respectively, of the 1D disordered waveguide. The figures display the output signal envelopes.

coincides with those of a first- and second-order differentiator, respectively. Wave-based signal processing holds the promise of being fast and energy efficient. Implementations of higher-order derivatives have been proposed mainly in carefully engineered static optical fiber systems [57–61]. Recently, Ref. [39] proposed to tune the scattering response of random overmoded scattering systems with many tunable degrees of freedom to CPA in order to perform metaprogrammable analog differentiation with unprecedented flexibility and fidelity; to implement higher-order differentiation, Ref. [39] cascaded two systems tuned to CPA in order to emulate the transfer function of a CPA EP. Here, by controlling the depth of the perturber penetration, we can tune our system to either an RL or RL-EP state. In the latter case, we implement the second-order differentiator transfer function without using any nonlinear components. For the prototypical example of a Gaussian input pulse, we calculate the envelopes of the output signal based on the measured transfer function for these two states. The results are displayed in Fig. 4 and in agreement with the analytically expected derivative. We attribute the imperfections to the fact that absorption prevents our RL EP from lying directly on the real axis.

In conclusion, we have observed the coalescence of RL states into EPs in regular and disordered single- and multichannel scattering systems. We have shown that, in symmetric systems where the spectrum can be modeled with two overlapping resonances, an RL EP requires that the spacing between two resonances is perfectly balanced by the coupling rate of symmetric and antisymmetric modes. An interesting extension of our work would consist in observing EPs related to transmissionless states [62] which theoretically provide the same behavior.

This publication was supported by the European Union through the European Regional Development Fund (ERDF), by the French region of Brittany and Rennes Métropole through the CPER Project SOPHIE/STIC & Ondes. M. D. acknowledges the Institut Universitaire de France. C. F. acknowledges funding from the French "Ministère de la Défense, Direction Générale de l'Armement." The data that support the plots within this Letter and other findings of this study are available from the corresponding authors on reasonable request.

*Corresponding author.
matthieu.davy@univ-rennes1.fr

[1] W. Heiss, Phys. Rev. E **61**, 929 (2000).
[2] M. V. Berry, Czech. J. Phys. **54**, 1039 (2004).
[3] I. Rotter, J. Phys. A **42**, 153001 (2009).
[4] N. Moiseyev, *Non-Hermitian Quantum Mechanics* (Cambridge University Press, Cambridge, England, 2011).
[5] H. Cao and J. Wiersig, Rev. Mod. Phys. **87**, 61 (2015).
[6] M.-A. Miri and A. Alu, Science **363**, eaar7709 (2019).
[7] Å. K. Özdemir, S. Rotter, F. Nori, and L. Yang, Nat. Mater. **18**, 783 (2019).
[8] Z. Lin, H. Ramezani, T. Eichelkraut, T. Kottos, H. Cao, and D. N. Christodoulides, Phys. Rev. Lett. **106**, 213901 (2011).
[9] R. Fleury, D. Sounas, and A. Alù, Nat. Commun. **6**, 5905 (2015).
[10] J. Doppler, A. A. Mailybaev, J. Böhm, U. Kuhl, A. Girschik, F. Libisch, T. J. Milburn, P. Rabl, N. Moiseyev, and S. Rotter, Nature (London) **537**, 76 (2016).
[11] B. Peng, Å. K. Özdemir, M. Liertzer, W. Chen, J. Kramer, H. Yilmaz, J. Wiersig, S. Rotter, and L. Yang, Proc. Natl. Acad. Sci. U.S.A. **113**, 6845 (2016).
[12] R. El-Ganainy, K. G. Makris, M. Khajavikhan, Z. H. Musslimani, S. Rotter, and D. N. Christodoulides, Nat. Phys. **14**, 11 (2018).
[13] W. Chen, S. Kaya Özdemir, G. Zhao, J. Wiersig, and L. Yang, Nature (London) **548**, 192 (2017).
[14] H. Hodaei, A. U. Hassan, S. Wittek, H. Garcia-Gracia, R. El-Ganainy, D. N. Christodoulides, and M. Khajavikhan, Nature (London) **548**, 187 (2017).
[15] A. Gorbatsevich and N. Shubin, Ann. Phys. (Amsterdam) **376**, 353 (2017).
[16] W. R. Sweeney, C. W. Hsu, and A. D. Stone, Phys. Rev. A **102**, 063511 (2020).
[17] A. D. Stone, W. R. Sweeney, C. W. Hsu, K. Wisal, and Z. Wang, Nanophotonics **10**, 343 (2021).
[18] W. R. Sweeney, C. W. Hsu, S. Rotter, and A. D. Stone, Phys. Rev. Lett. **122**, 093901 (2019).
[19] C. Wang, W. R. Sweeney, A. D. Stone, and L. Yang, Science **373**, 1261 (2021).
[20] A. A. Gorbatsevich and N. M. Shubin, JETP Lett. **103**, 769 (2016).
[21] A. A. Gorbatsevich and N. M. Shubin, Phys. Rev. B **96**, 205441 (2017).
[22] A.-S. Bonnet-Ben Dhia, L. Chesnel, and V. Pagneux, Proc. R. Soc. A **474**, 20180050 (2018).
[23] Y. D. Chong, L. Ge, H. Cao, and A. D. Stone, Phys. Rev. Lett. **105**, 053901 (2010).
[24] K. Pichler, M. Kühmayer, J. Böhm, A. Brandstatter, P. Ambichl, U. Kuhl, and S. Rotter, Nature (London) **567**, 351 (2019).
[25] S. Suwunnarat, Y. Tang, M. Reisner, F. Mortessagne, U. Kuhl, and T. Kottos, Commun. Phys. **5**, 5 (2022).

[26] H. Li, S. Suwunnarat, R. Fleischmann, H. Schanz, and T. Kottos, Phys. Rev. Lett. **118**, 044101 (2017).
[27] Y. V. Fyodorov, S. Suwunnarat, and T. Kottos, J. Phys. A Math. **50**, 30LT01 (2017).
[28] D. G. Baranov, A. Krasnok, T. Shegai, A. Alù, and Y. Chong, Nat. Rev. Mater. **2**, 17064 (2017).
[29] A. Krasnok, D. Baranov, H. Li, M.-A. Miri, F. Monticone, and A. Alù, Adv. Opt. Photonics **11**, 892 (2019).
[30] T. Roger, S. Vezzoli, E. Bolduc, J. Valente, J. J. F. Heitz, J. Jeffers, C. Soci, J. Leach, C. Couteau, N. I. Zheludev, and D. Faccio, Nat. Commun. **6**, 7031 (2015).
[31] J. R. Piper, V. Liu, and S. Fan, Appl, Phys. Lett. **104**, 251110 (2014).
[32] W. Wan, Y. Chong, L. Ge, H. Noh, A. D. Stone, and H. Cao, Science **331**, 889 (2011).
[33] M. F. Imani, D. R. Smith, and P. del Hougne, Adv. Funct. Mater. **30**, 2005310 (2020).
[34] L. Chen, T. Kottos, and S. M. Anlage, Nat. Commun. **11**, 1 (2020).
[35] B. W. Frazier, T. M. Antonsen Jr, S. M. Anlage, and E. Ott, Phys. Rev. Research **2**, 043422 (2020).
[36] P. del Hougne, K. B. Yeo, P. Besnier, and M. Davy, Laser Photonics Rev. **15**, 2000471 (2021).
[37] P. del Hougne, K. B. Yeo, P. Besnier, and M. Davy, Phys. Rev. Lett. **126**, 193903 (2021).
[38] L. Chen, S. M. Anlage, and Y. V. Fyodorov, Phys. Rev. E **103**, L050203 (2021).
[39] J. Sol, D. R. Smith, and P. del Hougne, Nat. Commun. **13**, 1713 (2022).
[40] S. Butterworth, Wirel. Eng. **7**, 536 (1930).
[41] V. K. Aatre, *Network Theory and Filter Design* (New Age International, New Delhi, 1986).
[42] H. Van de Stadt and J. M. Muller, J. Opt. Soc. Am. A **2**, 1363 (1985).
[43] J. Stone, L. Stulz, and A. Saleh, Electron. Lett. **26**, 1073 (1990).
[44] M. Stephen, M. Fahey, and I. Miller, Appl. Opt. **56**, 2636 (2017).
[45] Y. S. Joe, D. S. Ikeler, R. M. Cosby, A. M. Satanin, and C. Sub Kim, J. Appl. Phys. **88**, 2704 (2000).
[46] H.-W. Lee and C. S. Kim, Phys. Rev. B **63**, 075306 (2001).
[47] See Supplemental Material at http://link.aps.org/supplemental/10.1103/PhysRevLett.128.203904 for details on the experimental setups and the modal analysis, which includes Refs. [48–50].
[48] V. A. Mandelshtam and H. S. Taylor, J. Chem. Phys. **107**, 6756 (1997).
[49] M. Davy and A. Z. Genack, Phys. Rev. Research **1**, 033026 (2019).
[50] C. Poli, O. Legrand, and F. Mortessagne, Phys. Rev. E **82**, 055201(R) (2010).
[51] U. Kuhl, R. Höhmann, J. Main, and H. J. Stöckmann, Phys. Rev. Lett. **100**, 254101 (2008).
[52] M. Davy and A. Z. Genack, Nat. Commun. **9**, 4714 (2018).
[53] M. Cotrufo, E. Verhagen, and A. Fiore, in *Quantum Sensing and Nano Electronics and Photonics XIV, SPIE OPTO, 2017, San Francisco, California, USA* (International Society for Optics and Photonics), Vol. 10111. p. 1011128, 10.1117/12.2252037.
[54] K. G. Cognée, W. Yan, F. La China, D. Balestri, F. Intonti, M. Gurioli, A. F. Koenderink, and P. Lalanne, Optica **6**, 269 (2019).
[55] M. Davy, Z. Shi, J. Park, C. Tian, and A. Z. Genack, Nat. Commun. **6**, 6893 (2015).
[56] M. Davy, M. Kühmayer, S. Gigan, and S. Rotter, Commun. Phys. **4**, 85 (2021).
[57] N. Ngo, S. F. Yu, S. Tjin, and C. Kam, Opt. Commun. **230**, 115 (2004).
[58] C.-W. Hsue, L.-C. Tsai, and K.-L. Chen, IEEE Trans. Microwave Theory Tech. **52**, 1443 (2004).
[59] M. Kulishov and J. Azaña, Opt. Lett. **30**, 2700 (2005).
[60] Y. Park, J. Azaña, and R. Slavík, Opt. Lett. **32**, 710 (2007).
[61] M. Li, D. Janner, J. Yao, and V. Pruneri, Opt. Express **17**, 19798 (2009).
[62] Y. Kang and A. Z. Genack, Phys. Rev. B **103**, L100201 (2021).